2023-03-14

A Model for Multi-Input Mechanical Advantage in Origami-Based Mechanisms

Jared Butler
Brigham Young University - Provo

Adam Shrager
Pennsylvania State University

Timothy Simpson
Brigham Young University - Provo

Landen Bowen
Pennsylvania State University

Mary Frecker
Pennsylvania State University

See next page for additional authors

Original Publication Citation

Butler, J., Bowen, L., Wilcox, E., Shrager, A., Frecker, M. I., von Lockette, P., Simpson, T. W., Lang, R. J., Howell, L. L., and Magleby, S. P. (September 17, 2018). "A Model for Multi-Input Mechanical Advantage in Origami-Based Mechanisms." ASME. J. Mechanisms Robotics. December 2018; 10(6): 061007. https://doi.org/10.1115/1.4041199

A Model for Multi-Input Mechanical Advantage in Origami-Based Mechanisms*

Jared Butler
Dept. of Mechanical Engineering
Brigham Young University
Provo, UT, 84602

Landen Bowen
Dept. of Mechanical Engineering
Pennsylvania State University
University Park, PA 16802

Eric Wilcox
Dept. of Mechanical Engineering
Brigham Young University
Provo, UT, 84602

Adam Shrager
Dept. of Mechanical Engineering
Pennsylvania State University

Mary Frecker
Dept. of Mechanical Engineering
Pennsylvania State University
University Park, PA 16802

Paris von Lockette
Dept. of Mechanical Engineering
Pennsylvania State University
University Park, PA 16802

Timothy Simpson
Dept. of Mechanical Engineering
Pennsylvania State University
University Park, PA 16802

Robert Lang
Lang Origami
Alamo, CA 94507

Larry Howell
Dept. of Mechanical Engineering
Brigham Young University
Provo, UT 84602

Spencer Magleby†
Dept. of Mechanical Engineering
Brigham Young University
Provo, UT 84602

Mechanical advantage is traditionally defined for single input and single-output rigid-body mechanisms. A generalized approach for identifying single-output mechanical advantage for a multiple-input compliant mechanism, such as many origami-based mechanisms, would prove useful in predicting complex mechanism behavior. While origami-based mechanisms are capable of offering unique solutions to engi neering problems, the design process of such mechanisms is complicated by the interaction of motion and forces. This paper presents a model of the mechanical advantage for multi input compliant mechanisms and explores how modifying the parameters of a model affects their behavior. The model is used to predict the force-deflection behavior of an origami based mechanism (Oriceps) and is verified with experimental data from magnetic actuation of the mechanism.

NOMENCLATURE

MA_r Rigid-body mechanical advantage
MA_c Mechanical advantage of a compliant mechanism

*Portions of this work were presented at IDETC 2015 as paper number 47708

†Corresponding author, magleby@byu.edu

U_c Strain energy
W_{in} Input work
δU_c Differential change in strain energy
δW_{in} Differential change in input work
q Generalized coordinate
α_i Sector angle (spherical link length)
γ_i Exterior dihedral angle
k_i Torsional stiffness of a compliant hinge
V Volume
m Remanent magnetization

H Applied magnetic field strength (T)

E Modulus of elasticity

I Area moment of inertia

l Flexure length

t Material thickness

w Flexure width

L_1 Distance from the tip to the base of the Oriceps' jaw δW_L Differential input work at the Oriceps jaws

δW_s Differential input work at the Oriceps side panels

F_{out} Output force from Oriceps

1

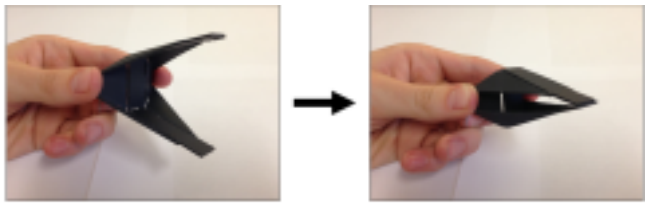

Fig. 1. Oriceps being actuated.

1 Introduction

Mechanical advantage can be useful in predicting force outputs in a mechanism. Mechanical advantage is traditionally defined for single-input and single-output rigid-body mechanisms. Less defined is the mechanical advantage of multiple-input compliant mechanisms, such as systems with multiple actuators, applied loads, or dynamic loading. While models for compliant mechanical advantage have been developed [1], a generalized approach for identifying single output mechanical advantage for a multiple-input compliant mechanism would prove useful in predicting complex mechanism behavior, such as that found in origami-based mechanisms.

Origami-based mechanisms are a type of compliant mechanism that potentially offer unique solutions to engi neering problems, having found application in the medical field [2–6], aerospace technology [7–9], aircraft construc tion [10–12], batteries [13], and robotics [14–20]. Origami can enable the design of mechanisms that change shape to meet practical requirements [21] or to construct mechanical meta-materials [22]. While the use of origami-based mechanisms can be attractive to designers, the design process is complicated by the interaction of motion and forces. Understanding transmission of forces within origami-based compliant mechanisms is challenging due to complex kinematics, inherent stiffness in joints, damping, and multi-input actuation. This understanding is particularly important when a mechanism is required to perform a mechanical task beyond simply achieving a desired folding motion – requiring spe cific force-deflection behavior and force output.

One recently proposed origami-based mechanism is the forceps known as the Oriceps [23], shown in Figure 1. The Oriceps are an example of action origami, origami designed to exhibit motion in its folded state [24]. The Oriceps have the potential to be an inexpensive and scalable alternative to current forceps used in the medical industry. The Oriceps can be fabricated from a single flat sheet of material, deployed from a planar configuration to an operating configuration, and are capable of producing a clamping motion, as seen in Figure 1.

The objective of this paper is to develop a model that can predict multi-input mechanical advantage in complex compliant mechanisms. This model will be used to predict the force-deflection behavior of an origami-based mechanism, specifically the Oriceps. The model is verified by

Fig. 2. Oriceps fold pattern. Solid lines represent valley folds, while dotted lines represent mountain folds.

Fig. 3. Open and closed positions of the Oriceps.

2 Background

2.1 Mechanical Advantage

Mechanical advantage has been traditionally used to predict single output forces in a rigid-body mechanism and is found by comparing the output force to the input force as:

$$MA = \frac{||F_o||}{||F_i||} \quad (1)$$

The mechanical advantage of a rigid-body mechanism can also be viewed as a function of differential change in position of the input with respect to the output of the mechanism:

$$MA = \frac{ds_i}{ds_o} \quad (2)$$

Previous work has identified the mechanical advantage of rigid-body mechanisms when multiple parameters within the model are discussed and their effects on performance are explored. experimental data gathered from magnetic actuation of the Oriceps. Key

where δU_c is the differential change in strain energy due to compliance in the mechanism and $\delta d_i F_i$ is the differen tial change in distance multiplied by the input force. Equation 3 defines the compliant mechanical advantage MA_c as a proportion of the mechanical advantage of a mechanism's rigid-body motion MA_r. This form of compliant mechanical advantage will serve later in the paper as the conduit to creating a model to predict mechanism behavior with multiple inputs to the system.

2.2 Oriceps

The Oriceps, shown in Figure 1, were inspired by the "Chomper," an origami model designed by Jeremy Shafer [27]. The Chomper is capable of opening and closing its "mouth" as a result of several simple folds in a flat sheet. The Oriceps were developed by modifying the Chomper to create a simplified fold pattern that folded more compactly while maintaining a wide gripping surface [23]. A general Oriceps fold using a single sheet of material and planar manufacturing processes, they can be produced inexpensively, potentially replacing traditional for form is shown in its open and closed positions in Figure 3. Because the Oriceps can be fabricated

The Oriceps achieve their motion by localized bending about crease lines while the panels remain planar, meaning they fall into the category of rigidly foldable origami. Because most of the displacement is a result of deforma tion at the crease lines, they can be modeled by compliant hinges that act as surrogates for the origami folds. Therefore, the Oriceps can be considered a compliant mechanism, and the flexing at the creases can be modeled with small-length flexural pivots, with properties promising method of actuation, particularly with the application of the Oriceps as a minimally-invasive surgical tool where the actuation method

2.3 Active Materials for Actuation

Active materials represent a

output forces are desired in a mechanism [25].

Compliance in a mechanism increases the complexity of accurately modeling its mechanical advantage. Strain within the mechanism reduces the expected output forces [26]. Sala mon and Midha [1] developed a form for mechanical advan tage in a traditional single-input and single-output compliant mechanism, defined by:

$$MA_c = MA_r \quad (3)$$

$$\frac{1 - \delta U_c}{\delta d_i F_i}$$

2

pattern is depicted in Figure 2, and the folded

Fig. 4. Mechanical advantage model of the Oriceps (reduced by symmetry). Input (blue, light) and output (red, dark) moments are indicated.

mechanical advantage at a single output. The denominator term in Equation 3 represents the differential change in input work to the system, allowing Equation 3 to be written as:

ceps with a disposable alternative.

$$MA_c = MA_r \quad \frac{1 - \delta U_c}{\delta W_{in}} \quad (4)$$

determined using compliant mechanism theory [28].

In this form, it is observed that the ratio of differential change in strain energy δU_c to differential change in input work δW_{in} dictates how much the compliance of the system affects the mechanical advantage.

Equation 4 accommodates any strain within the system. Differential strains within the system must all be defined with respect to the same generalized coordinate q. Doing so pro vides a generalized form for the net differential strain within the mechanism:

$$\delta U_c = \frac{\sum_{i=1}^{n} dU_{c,i}}{dq} \delta q \quad (5)$$

must also be as compact as possible [23]. There have been many proposed methods for the actuation of origami-based designs using active materials, including light-responsive polymers [29,30], dielectric elastomers [31–34], electrothermal actuators [35], magnetics [36–40], and shape memory alloys [41, 42]. A table comparing key metrics of these actuation methods is available in [43]. As magnetically active materials (both permanent magnets and magneto-active elas tomers) are capable of both large actuation forces and bi directional actuation [43, 44], permanent magnets were chosen as the actuation method for the active Oriceps used in paper. 3 Mechanical

verification testing for this

While mechanical advantage is traditionally defined by single-input and single-output mechanisms, Equation 3 can be generalized to accommodate multiple inputs to find the Advantage Model

The same approach may be used to accommodate mul tiple inputs within the system. Any number of points on the mechanism may have work performed on them to affect the output force. Using differential work as the input to the system removes the complexity of accommodating inputs about varying directions if the differential change in work is determined with respect to the generalized coordinate q. Doing so provides a δW_{in} as:

$$\delta W_{in} = \sum_{i=1}^{n} \frac{dW_{in,i}}{dq} \delta q \quad (6)$$

advantage of a compliant mechanism at any given configuration with considerations for system strain and multiple inputs.

3

Equations 4 – 6 will predict the mechanical

relations may be found [45]:

γ_1

General relationships exist for the dihedral angles of degree-4 vertices. In the special case where:

$$\alpha_1 + \alpha_2 = \alpha_3 + \alpha_4 = \pi \quad (7)$$

$$\gamma_3 = -\gamma_1 \quad (8)$$

which applies to the Oriceps, the following

α_1 α_4

α_2 α_3

γ_2

γ_3

$$\gamma_4 = -2\arccot\left(\frac{2\cot(\frac{\gamma_1}{2})\csc\alpha_1}{(1-\cot^2(\frac{\gamma_1}{2}))\cot\alpha_1 + (1+\cot^2(\frac{\gamma_1}{2}))\cot\alpha_3}\right)$$

$$\gamma_2 = 2\arccot\left(\frac{2\cot(\frac{\gamma_1}{2})\csc\alpha_3}{(1-\cot^2(\frac{\gamma_1}{2}))\cot\alpha_3 + (1+\cot^2(\frac{\gamma_1}{2}))\cot\alpha_1}\right) \quad (9)$$

Fig. 5. Partially folded vertex within the Oriceps with sector angles (α) and exterior dihedral angles (γ) shown. The ground link (α_3) is indicated with hatched lines.

4 Oriceps Model

4.1 Assumptions

The use of magnets as a means of actuation introduces additional complexity to the Oriceps model.

(10)

The exterior dihedral angle γ is a measure of the devia tion from flatness of the angle

between two panels such that its value is 0° when the panels are in their planar position and ± 180° when fully folded.

For this vertex, the driving angle is γ_3, and the output is the angular deflection of γ_4. Using Equation 8, Equations 9 and 10 can be re-written in terms of γ_3:

$$\gamma_2 = 2\operatorname{arccot}\left(\frac{\sin\alpha_1\cot\alpha_1(\cot^2(\frac{\gamma_3}{2})-1)-\cot\alpha_3(\cot^2(\frac{\gamma_3}{2})+1)}{2\cot(\frac{\gamma_3}{2})}\right) \quad (11)$$

$$\gamma_4 = -2\operatorname{arccot}\left(\frac{\sin\alpha_3\cot\alpha_1(\cot^2(\frac{\gamma_3}{2})+1)-\cot\alpha_3(\cot^2(\frac{\gamma_3}{2})-1)}{2\cot(\frac{\gamma_3}{2})}\right) \quad (12)$$

While developing the model of the Oriceps, several assumptions were made for the behaviors of the Oriceps and the magnets. These assumptions make the analysis and equations more useful for design as the generalized equations can quickly become complex and difficult to use. The Oriceps are assumed to be rigid foldable, meaning all motion is assumed to be achieved through localized flexing at the fold lines without any deflection of the panels. The panels themselves are assumed to be massless. The compliant hinges which connect the panels are assumed to have constant bending stiffnesses.

The magnets used for actuation are assumed to have negligible interaction with each other and the applied magnetic field within the immediate proximity of the Oriceps is assumed to be constant and uniform.

4.2 Rigid-Body Motion

Due to symmetry, all vertices within the Oriceps are identical, reducing the analysis to a single vertex which can be represented as a 1 degree-of-freedom spherical mechanism, as shown in Figure 4. Here the center panel (α_3) was considered as ground with actuation input (blue) and output (red) acting about γ_3 and γ_4 respectively. The partially folded vertex is shown in Figure 5 with sector angles (α_i) and exterior dihedral angles (γ_i) indicated.

With the input and output assigned, Equation 2 can be used to define the mechanical advantage of a rigid-body equivalent of the vertex as:

$$MA_r = \frac{d\gamma_3}{d\gamma_4} \quad (13)$$

which is given explicitly as:

$$MA_r = \frac{4[\cos(\alpha_3)\cos(\gamma_3)-\cot(\alpha_1)\sin(\alpha_3)]^2}{+\sin^2(\gamma_3) -2\cos(\alpha_3) +2\cos(\gamma_3)\cot(\alpha_1)\sin(\alpha_3)} \quad (14)$$

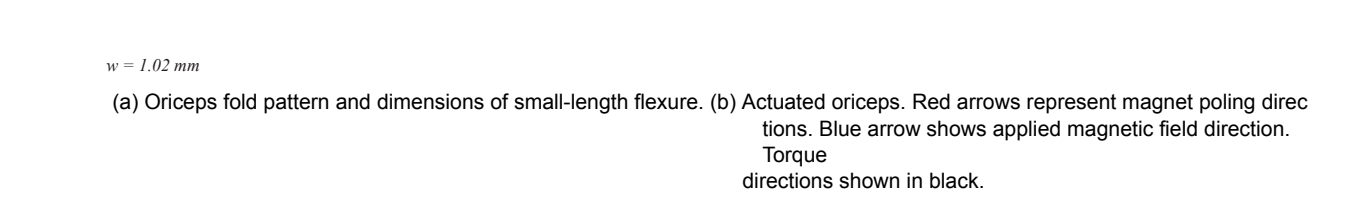

(a) Oriceps fold pattern and dimensions of small-length flexure. (b) Actuated oriceps. Red arrows represent magnet poling directions. Blue arrow shows applied magnetic field direction. Torque directions shown in black.

Fig. 6. Oriceps fold pattern with placement of the magnets and their respective poling directions.

4.3 Considerations for Compliance

Under the assumption that a rigidly-foldable mechanism restricts deflection to only the creases, the strain energy within the Oriceps and any other rigidly-foldable origami mechanism can be given by:

$$B = \mu_o H \quad (18)$$

and M is given by:

of free space μ_o as:

$$U_c = \sum_{i=1}^{n} \frac{1}{2} k_i (\gamma_i - \gamma_{io})^2 \quad (15)$$

with γ_{io} representing the angle between panels in the vertex's resting state and stiffness represented by k_i.

The differential change in strain energy δU_c must be taken with respect to the generalized coordinate. The driv ing angle γ_3 was selected as the generalized coordinate for the Oriceps, yielding:

$$\delta U_c = \sum_{i=1}^{n} k_i (\gamma_i - \gamma_{io}) d\gamma_i \quad (16)$$

For use on the Oriceps, input work was provided by interactions between magnetic fields. Permanent magnets of two sizes [46] were mounted to the panels of the fold pattern as shown in Figure 6. Each magnet has a specific poling direction and, when placed in a magnetic field, these magnets align to the field. The applied torque due to the magnetic fields is given by [47]:

$$W_{in} = \sum_{i=1}^{4} N (\gamma_i - \gamma_{io}) \quad (21)$$

$$N = M \times B \quad (17)$$

where N is the torque, M is the magnetic dipole moment, and B is the applied magnetic field. B is equivalent to the product of the applied magnetic field strength H and the permeability

$$M = Vm \quad (19)$$

where m is the magnet's remanent magnetization (specified by the manufacturer as 1.32 T) and V is the volume of the magnet (63.9 mm^3). Substituting these values into Equation 17 removes μ_o from the equation and yields:

$$N = Vm \times H \quad (20)$$

As the Oriceps move through the magnetic field, the magnets perform work on the panels to which they are mounted. The magnitude of the torques can be used to find the applied work on the Oriceps as:

where N is the torque magnitude of a given magnet. Equation 21 can be differentiated with respect to the generalized coordinate γ_3 to provide the differential change in input work at a given configuration:

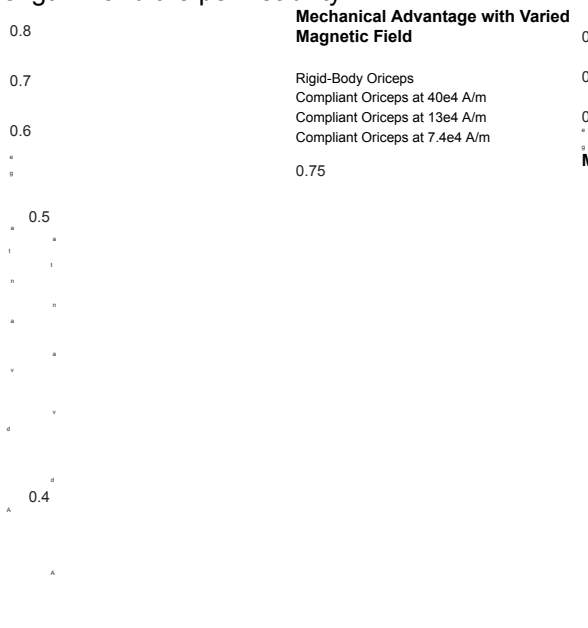

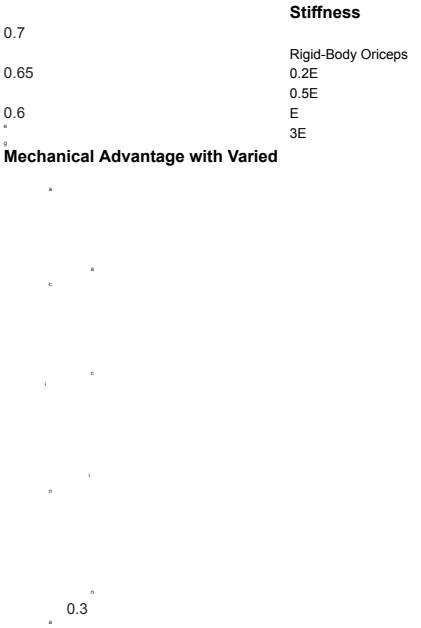

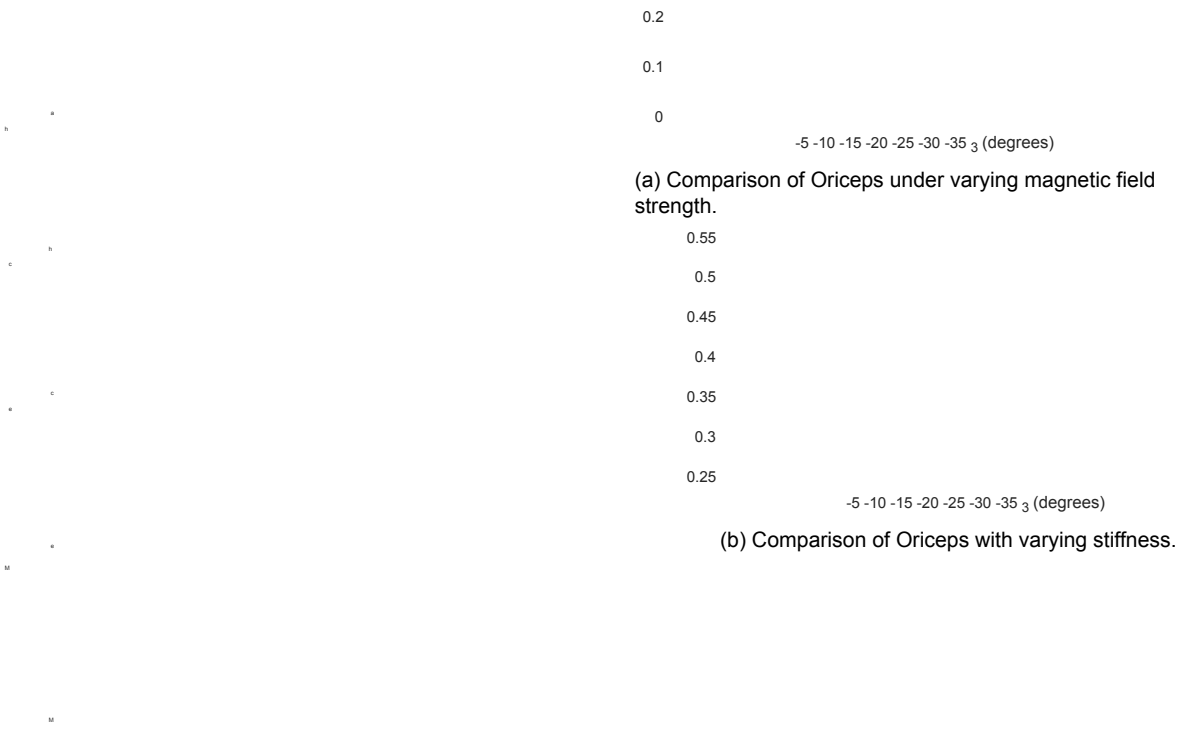

(a) Comparison of Oriceps under varying magnetic field strength.

(b) Comparison of Oriceps with varying stiffness.

Fig. 7. Comparison of degree-4 vertex theoretical mechanical advantage profiles throughout actuation for the rigid-body Oriceps and the compliant Oriceps. The stiffness in (b) is varied by changing the modulus of elasticity, where E represents the modulus for the design in (a).

$$\delta W_{in} = \sum_{i=1}^{4} N d\gamma_i \, d\gamma_3 \delta\gamma_3 \quad (22)$$

5 Determining Mechanical Advantage in Oriceps

Using the multi-input compliant mechanical advantage model developed in Sections 3 and 4, the mechanical advantage of the fabricated Oriceps throughout actuation was calculated and predicted. This analysis was done by substi tuting values from the geometry and actuation parameters of the specified design.

5.1 Fabrication

The Oriceps used in testing were laser cut from a 0.43 mm (0.017 in) thick sheet of Formex® flame retardant polypropylene using the dimensions given in Table 1. Lightweight rigid material was attached to the panels comprising the jaws so that they would not deform locally during actuation. The magnets attached to the Oriceps, shown in Figure 6, were of two dimensions. Magnets attached to the left and right panels are of dimension 6.35 mm x 6.35 mm x 1.59 mm (0.250” x 0.250” x 0.0625”), and those in the center of 3.18 mm x 3.18 mm x 6.35 mm (0.125” x 0.125” x 0.250”). In its planar state, the Oriceps are at a change point. Therefore, the mechanism was initially actuated until its stable resting configuration was at $\gamma_{3o} = 5^{o}$.

$$k_i = EI_i \quad I_i \quad (23)$$

where E is the material’s modulus of elasticity, I the area moment of inertia of the flexure being considered, and l the

5.2 Compliant Hinge Stiffness

The Pseudo-Rigid-Body Model (PRBM) [28] can be used to predict the stiffness of a small-length flexure as:

length of the flexure. Using the experimentally measured geometry and approximate modulus of elasticity (150 MPa) of the Oriceps, each hinge stiffness was calculated, resulting in 4.4×10^{-4} N-m/radian for k_1 and k_2 and 2.2×10^{-4} N m/radian for k_3 and k_4.

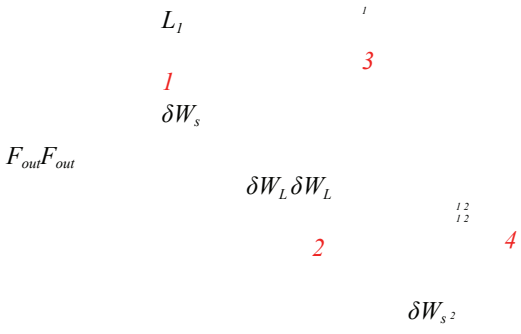

Fig. 8. Oriceps fold pattern with vertices numbered 1-4, actuation inputs, and force outputs.

5.3 Predicted Behavior

Figure 7 compares theoretical mechanical advantages of the Oriceps under varying conditions. The solid blue line in each plot indicates the mechanical advantage of a rigid body Oriceps consisting of rigid panels with hinges. The

Table 1. Specific geometry of the Oriceps from which experimental data was gathered.

Geometry	Value
α_1	$\frac{2\pi}{3}$
α_2	$\frac{\pi}{3}$
α_3	$\frac{\pi}{2}$
α_4	$\frac{\pi}{2}$
t	0.43 mm (0.017 in)
w	1.02 mm (0.040 in)
l	1.52 mm (0.060 in)
L_1	23.62 mm (0.93 in)

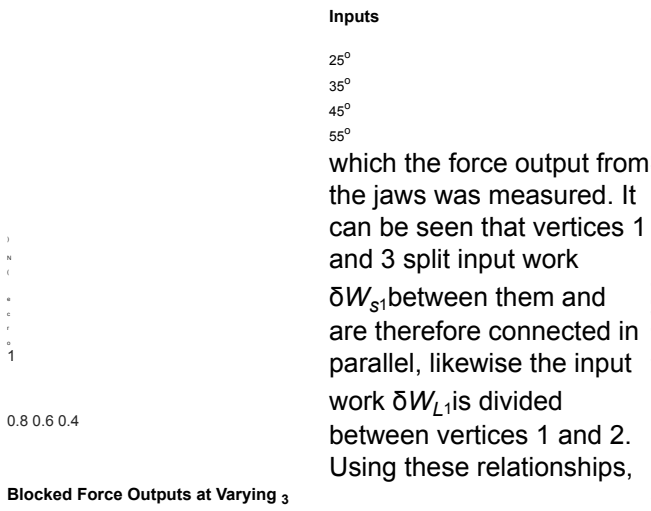

Fig. 9. Predicted blocked force output at varying values of γ_3.

other lines show the mechanical advantages of a compliant hinged Oriceps under varying magnetic field strength (Figure 7(a)) and under varying hinge stiffness (Figure 7(b)). Figure 7(a) shows that as the magnetic field used to actuate the Oriceps is increased, the predicted compliant mechanical advantage approaches that of the rigid-body Oriceps. Figure 7(b) shows that as hinge stiffness decreases, the predicted compliant mechanical advantage also approaches that of the rigid-body Oriceps. This supports the expected result from Equation 4. If δW_{in} becomes much larger than δU_c, MA_c approaches MA_r.

Throughout actuation, compliance in the hinges requires more input energy, decreasing the mechanical advantage. As the actuation angle increases, the difference in mechanical advantage between the rigid-body Oriceps and the compliant Oriceps increases. Figure 7 shows the increasing difference in mechanical advantage throughout actuation, qualitatively verifying the expected behavior of the compliant Oriceps.

6 Force Output

6.1 Force Output Model

Figure 8 shows a schematic of the Oriceps with the locations of the multiple inputs from the magnets, the vertices in the fold pattern (numbered 1-4), and the locations from which the force output from the jaws was measured. It can be seen that vertices 1 and 3 split input work δW_{s1} between them and are therefore connected in parallel, likewise the input work δW_{L1} is divided between vertices 1 and 2. Using these relationships, the force output at the tip of the jaw is calculated to be:

$$F_{out1} = \text{where:}$$

$$h_{\delta W}{}^{s}{}_{1}$$

$$_{2}(MA_2) + {}^{\delta W_{L_1}}$$

$$_{2}(MA_1) + {}^{\delta W_{s_2}}$$

$$_{2}(MA_1) + {}^{\delta W_{L_2}}$$

$$_{2}(MA_2)$$

$$L^{1} \quad (24)$$

δW_{s1}= differential input work applied to input panel 1 δW_{s2}= differential input work applied to input panel 2 δW_{L1}= differential input work applied to output panel 1 δW_{L2}= differential input work applied to output panel 2 MA_1 = compliant mechanical advantage of vertex 1 MA_2 = compliant mechanical advantage of vertex 2 L_1 = length of the Oriceps jaws

Due to the equivalency of δW_{s1} with δW_{s2}, δW_{L1} with δW_{L2}, and MA_1 with MA_2, Equation 24 can be reduced to:

$$F_{out1} = MA_1 \, (\delta W_{s1} + \delta W_{L2}) \qquad L_1 \quad (25)$$

Using Equation 25, the force output from the Oriceps can be calculated. Figure 9 presents the expected force outputs at different fixed values of γ_3 as the applied magnetic field strength is increased. At a fixed angle, the output force responds linearly to the applied magnetic field as expected. Greater values of γ_3 have a lower relative output force at lower field strength. However, as field strength is increased, the mechanical advantage approaches that of the rigid-body model, allowing for the output force at greater values of γ_3 to exceed those of lesser values.

Fig. 10. Experimental setup to test force output during magnetic actuation.

Fig. 11. Oriceps being actuated in an applied magnetic field. Poling directions of each magnet are indicated with red (dark) arrows and the magnetic field with blue (light) arrows.

6.2 Testing

Figure 10 shows the full test setup with the voltage source, the electromagnet used to generate the magnetic field, and the force transducer used to measure the force generated by the Oriceps. The Oriceps were placed in a magnetic field as shown in Figure 11, and the blocked force (reaction force at zero displacement) was measured at differ ent magnetic field strengths. The electromagnet supplying the magnetic field is a C-shaped magnet fabricated in-house for lab use. The separation distance is 37.5 mm from pole face to pole face. The pole faces are 38.1 x 50.8 mm^2. The magnet consists of approximately 400 turns over approximately 100 mm in length and is driven by a Circuit Specialist CSI6030 0-60V/0-30A Bench Power Supply yielding a maximum field of approximately $\mu_0 H'$ 140 mT. The vertically directed field generated by the electromagnet in the volume between the pole faces has been mapped experimentally using a Lakeshore Gaussmeter, with a resolution of 0.01 mT, to measure field and a 3-axis position stage, with 0.1mm reso lution, to traverse the horizontal and vertical planes. The applied field, H, within the volume of the pole faces varies by a maximum of 7.4% vertically and 4.3% horizontally when working 5 mm away from the perimeter of the pole faces, as was done in the conduct of these experiments. This scal ing holds across the range of fields strengths tested in the manuscript.

When testing the blocked force, the Oriceps were con strained at $\gamma_3 = 35 \pm 2^\circ$ to ensure no motion as the magnetic field was varied. To measure the grip strength, one of the jaw tips was attached to a force transducer (IMADA DS2-1, 0-5 N range) with monofilament line. The magnet is calibrated so that the strength of the magnetic field can be determined as a function of voltage. Note that the electromagnet produces a small magnetic field of about 0.014 T even when there is no voltage applied. As the magnetic field was incrementally increased, the measured force was recorded and a digital image was taken to determine the angle of the monofilament line. Tests were repeated five separate times. From this data the component of force perpendicular to the jaw and the standard deviation for the sampled data was calculated.

6.3 Results

Figure 12 presents the results of the testing compared against the force output predicted by the developed model. Five tests were taken and the standard deviation of those results are plotted in the figure. It is shown that both the model and experimental data follow an approximately linear response. A minimum field strength of roughly 8.0e4 A/m was required to produce a measurable output force. At 7.4e4 A/m, the Oriceps remained static, producing no output force. Any field strength lower than 7.4e4 A/m would be insufficient to overcome the strain in the system, resulting in an output force in the opposite direction of the blocked force. This correlates with the predicted values of the output force which become negative if the magnetic field strength drops below 6.8 A/m, meaning the Oriceps will attempt to actuate outwards rather than inwards due to the strain energy in the deflected creases.

7 Discussion

The model can be considered more generally to give in sight on the parameters controlling the force-deflection behavior of the Oriceps. The key parameters of the analytical

Fig. 12. Calculated blocked force output at $\gamma_3 = 35^\circ$ as compared to experimental data. The standard deviation of sampled points are represented with error bars.

model under consideration are: δW_{in}, the input driving the motion of the mechanism, k, the hinge stiffness about the fold axis, and α, the sector angles of the panels.

7.1 Actuation Input

When compliant hinges are used in a mechanism, a por tion of the actuation input goes into the flexing of the compliant segments, reducing the overall force transmitted to the output. In a fixed configuration, the input energy must be greater than the energy required to flex the compliant segments from its resting position to its fixed position to produce an output gripping force. Once the input energy becomes equivalent to the energy required to flex the compliant segments to the fixed position, the mechanical advantage of the mechanism is zero, reducing the force output to zero.

In applications where the magnitude of the driving input is large relative to the stiffness of the compliant hinges with zero stiffness, which (by at least an order of magnitude), simplifies the analysis of the the mechanical advan tage of the mechanism. compliant mechanism will closely approximate that of its rigid-body equivalent. In such cases, the Oriceps could be modeled as having

$$\sum_{i=1}^{n}$$

hinges of actuation up to $\gamma_3 = 35^\circ$. Once the mechanical advantage reaches zero, the output force and motion also become zero, occurring when:

$$\delta W_{in} = \delta U_c \quad (26)$$

If the actuation input is limited below a maximum, $\delta W_{in_{max}}$, then a critical stiffness value for a desired range of motion (assuming all hinges have identical stiffness), k_{crit}, can be given as:

$$k_{crit} = \frac{\delta W_{in_{max}}}{}$$

7.3 Sector Angles

$$\frac{d\gamma_3}{(\gamma_i - \gamma_{io})^{d\gamma_i}} \delta\gamma_3 \quad (27)$$

7.2 Hinge Stiffness

When using compliant hinges in an origami-based design, each hinge can be modeled as a torsional spring with an associated stiffness. Modifying the hinges to change their torsional stiffness can significantly affect the mechanical advantage of the mechanism.

Compliant hinge stiffness is directly correlated to both the output force of the mechanism and the available range of motion under a given input. As seen in Figure 7, the Oriceps under actuation of a 7.4*e*4 A/m field strength is only capable

The mechanical advantage can be altered by modifying the sector angles (spherical link lengths) of the vertex. The theoretical maximum mechanical advantage of a degree-4 vertex occurs when all the sector angles are $\frac{\pi}{2}$; however, a vertex with sector angles all equal to $\frac{\pi}{2}$ will no longer be fully coupled – meaning the vertex will fold sequentially (fold in half then fold in half again). If the vertex's sector angles approach this singularity, the range of motion is greatly reduced. When modifying the sector angles in the Oriceps, an optimum design will maximize mechanical advantage while maintaining a sufficient range of motion for an application.

9

8 Conclusion

This paper presents a model for calculating the mechan ical advantage of a multi-input compliant mechanism. The model has been verified through experimental data taken for an origami-based mechanism (i.e. the Oriceps). This model led to a discussion of key parameters affecting the force deflection behavior of the Oriceps.

In the development of any actuated origami-based mechanism, it is important to have a good understanding of the parameters controlling its force-deflection behavior, motion, and mechanical advantage. The mechanical advantage model and parameters described here enable designers to gain this critical understanding of the effect of design decisions on the functionality and actuation of the Oriceps.

Additionally, magnetically active materials (such as MAE) were demonstrated to create folding/unfolding motion in origami-based mechanisms. The application of active materials as actuators in origami-based mechanisms is desir able due to their compactness (relative to other conventional actuation techniques) and ability to be triggered without mechanical interaction (e.g., triggering motion through applied thermal, magnetic, or electric fields).

The model presented in this paper is applicable to compliant mechanisms where system motion can be modeled by hinges with stiffness to represent the resistance to motion. The approach applies to systems with greater thickness than what was demonstrated in the Oriceps, but different design approaches would be needed to accommodate for interfer ence between thick panels and to provide sufficient motion in the hinges. [48]

This paper demonstrated the possibility of creating predictive models that give designers insight into the behavior of an origami-based mechanism and parameters that control its performance. These predictive models will enable designers to overcome many of the challenges unique to origami based mechanisms and allow them to incorporate origami based design principles to overcome design challenges.

9 Acknowledgments

Thanks to Amanda Chennavasin, Daniel DePolo, Sarah Kelly, Reena Philips, Thomas Scully, and Eric Swartz for experimental setup and data acquisition. Thanks to Alex Avila and Jacob Badger for technical review. This paper is based on work supported by the National Science Foundation and the Air Force Office of Scientific Research through NSF Grant No. EFRI-ODISSEI-1240417 at Brigham Young University and EFRI-ODISSEI-1240459 at Pennsylvania State University.

References

[1] Salamon, B., and Midha, A., 1998. "An introduction to mechanical advantage in compliant mechanisms". *Journal of Mechanical Design, 120*(2), pp. 311–315.

[2] Zhou, L., Marras, A. E., Castro, C. E., and Su, H.-J., 2016. "Pseudorigid-body models of compliant dna origami mechanisms". *Journal of Mechanisms and Robotics, 8*(5), p. 051013.

[3] Miyashita, S., Guitron, S., Ludersdorfer, M., Sung, C. R., and Rus, D., 2015. "An untethered miniature origami robot that self-folds, walks, swims, and de grades". In Robotics and Automation (ICRA), 2015 IEEE International Conference on, IEEE, pp. 1490– 1496.

[4] Miyashita, S., Guitron, S., Yoshida, K., Li, S., Damian, D. D., and Rus, D., 2016. "Ingestible, controllable, and degradable origami robot for patching stomach wounds". In Robotics and Automation (ICRA), 2016 IEEE International Conference on, IEEE, pp. 909–916.

[5] Taylor, A., Miller, M., Fok, M., Nilsson, K., and Tse, Z. T. H., 2016. "Intracardiac magnetic

resonance imaging catheter with origami deployable mechanisms". *Journal of Medical Devices, 10*(2), p. 020957.

[6] Johnson, M., Chen, Y., Hovet, S., Xu, S., Wood, B., Ren, H., Tokuda, J., and Tse, Z. T. H., 2017. "Fabricating biomedical origami: a state-of-the-art review". *International Journal of Computer Assisted Radiology and Surgery*, pp. 1–10.

[7] Zirbel, S., Magleby, S., Howell, L., Lang, R., Thomson, M., and Trease, B., 2013. "Accommodating thickness in origami-based deployable arrays1". *Journal of Mechanical Design, 135*(11), October 3, p. 111005.

[8] Butler, J., Morgan, J., Pehrson, N., Tolman, K., Bate man, T., Magleby, S. P., and Howell, L. L., 2016. "Highly compressible origami bellows for harsh envi ronments". In ASME 2016 International Design Engineering Technical Conferences and Computers and Information in Engineering Conference.

[9] Qiao, Q., Yuan, J., Shi, Y., Ning, X., and Wang, F., 2017. "Structure, design, and modeling of an origami inspired pneumatic solar tracking system for the npu phonesat". *Journal of Mechanisms and Robotics, 9*(1), p. 011004.

[10] Miyashita, S., DiDio, I., Ananthabhotla, I., An, B., Sung, C., Arabagi, S., and Rus, D., 2015. "Fold ing angle regulation by curved crease design for self assembling origami propellers". *Journal of Mecha nisms and Robotics, 7*(2), p. 021013.

[11] Baranger, E., Guidault, P.-A., and Cluzel, C., 2011. "Numerical modeling of the geometrical defects of an origami-like sandwich core". *Composite Structures, 93*(10), pp. 2504 – 2510.

[12] Nojima, T., and Saito, K., 2006. "Development of newly designed ultra-light core structures". *JSME In ternational Journal Series A Solid Mechanics and Ma terial Engineering, 49*, pp. 38–42.

[13] Cheng, Q., Song, Z., Ma, T., Smith, B., Tang, R., Yu, H., Jiang, H., and Chan, C., 2013. "Folding paper-based lithium-ion batteries for higher areal energy densities". *Nano Letters, 13*, pp. 4969–4974.

[14] Firouzeh, A., and Paik, J., 2017. "An under-actuated origami gripper with adjustable stiffness joints for mul tiple grasp modes". *Smart Materials and Structures, 26*(5), p. 055035.

10

[15] Chen, Y., Lv, W., Li, J., and You, Z., 2017. "An ex tended family of rigidly foldable origami tubes". *Jour nal of Mechanisms and Robotics, 9*(2), p. 021002.

[16] Firouzeh, A., and Paik, J., 2015. "Robogami: A fully integrated low-profile robotic origami". *Journal of Mechanisms and Robotics, 7*(2), p. 021009.

[17] Zhang, K., Qiu, C., and Dai, J. S., 2016. "An exten sible continuum robot with integrated origami parallel modules". *Journal of Mechanisms and Robotics, 8*(3), p. 031010.

[18] Pagano, A., Yan, T., Chien, B., Wissa, A., and Taw fick, S., 2017. "A crawling robot driven by multi-stable origami". *Smart Mater. Struct, 26*(094007), p. 094007.

[19] Onal, C., I. Wood, R. J., and Rus, D., 2013. "An origami-inspired approach to worm robots". *IEEE Transactions on Mechatronics, 18*(2), pp. 430–438.

[20] Felton, S., Tolley, M., Demaine, E., Rus, D., and Wood, R., 2014. "A method for building self-folding machines". *Science, 345*(6197), August, pp. 644–646.

[21] Guang, C., and Yang, Y., 2018. "Single-vertex mul ticrease rigid origami with nonzero thickness and its transformation into deployable mechanisms". *Journal of Mechanisms and Robotics, 10*(1), p. 011010.

[22] Yang, Y., and You, Z., 2018. "Geometry of transformable metamaterials inspired by modular origami". *Journal of Mechanisms and Robotics*.

[23] Edmondson, B., Bowen, L., Grames, G., Magleby, S., Howell, L., and Bateman, T., 2013. "Oriceps: Origami inspired forceps". *ASME 2013 Conference on Smart Materials, Adaptive Structures and Intelligent Systems*.

[24] Bowen, L., Grames, C., Magleby, S., Lang, R., and Howell, L., 2013. "A classification of action origami as systems of spherical mechanisms". *Journal of Me chanical Design, 135*(11), October 8, p. 111008.

[25] Midha, A., Hall, A. S., Her, I., and Bubel, G., 1984. "Mechanical advantage of single-input and multiple output ports mechanical device". *Journal of Mech anisms, Transmissions, and Automation in Design, 106*(4), pp. 462–469.

[26] Wang, M. Y., 2009. "Mechanical and geometric advan tages in compliant mechanism optimization". *Frontiers of Mechanical Engineering in China, 4*(3), pp. 229– 241.

[27] Shafer, J., 2010. *Origami Ooh La La!* CreateSpace Independent Publishing Platform, Lexington, KY. [28] Howell, L. L., 2001. *Compliant mechanisms*. John Wi ley & Sons.

[29] Liu, Y., Boyles, J., Genzer, J., and Dickey, M., 2012. "Self-folding of polymer sheets using local light ab sorbtion". *Soft Matter*.

[30] Ryu, J., D'Amato, M., Cui, X., Long, K., Qi, H., and Dunn, M., 2012. "Photo-origami - bending and folding polymers with light". *Applied Physics Letters*.

[31] Sun, W., Liu, F., Ma, Z., Li, C., and Zhou, J., 2016. "Soft mobile robots driven by foldable dielectric elas tomer actuators". *Journal of Applied Physics, 120*(8), p. 084901.

[32] Ahmed, S., Lauff, C., Crivaro, A., McGough, K., Sheri

dan, R., Frecker, M., Lockette, P., Ounaies, Z.,

Simp son, T., Lien, J., and Strzelec, R., 2013. “Multi-field re sponsive origami structures: Preliminary modelling and experiments”. *Proceedings of the ASME 2013 Interna tional Design Engineering Technical Conferences*.

[33] Ahmed, S., Ounaies, Z., and Frecker, M., 2014. “In vestigating the performance and properties of dielec tric elastomer actuators as a potential means to actuate origami structures”. *Smart Materials and Structures, 23*(2014).

[34] McGough, K., Ahmed, S., Frecker, M., and Ounaies, Z., 2014. “Finite element analysis and validation of dielectric elastomer actuators used for active origami”. *Smart Materials and Structures, 23*(2014).

[35] Shigemune, H., Maeda, S., Hara, Y., Hosoya, N., and Hashimoto, S., 2016. “Origami robot: A self-folding paper robot with an electrothermal actuator created by printing”. *IEEE/ASME Transactions on Mechatronics, 21*(6), pp. 2746–2754.

[36] Bowen, L., Springsteen, K., Ahmed, S., Arrojado, E., Frecker, M., Simpson, T. W., Ounaies, Z., and von Lockette, P., 2017. “Design, fabrication, and modeling of an electric–magnetic self-folding sheet”. *Journal of Mechanisms and Robotics, 9*(2), p. 021012.

[37] Cowan, B., and von Lockette, P. R., 2017. “Fabrication, characterization, and heuristic trade space exploration of magnetically actuated miura-ori origami structures”. *Smart Materials and Structures, 26*(4), p. 045015.

[38] Crivaro, A., Sheridan, R., Frecker, M., Simpson, T. W., and Von Lockette, P., 2016. “Bistable compliant mech anism using magneto active elastomer actuation”. *Jour nal of Intelligent* dation of the large deformation bending and folding be havior of magneto-active elastomer composites”. *Smart Materials and Structures, 23*(2014).

[45] Lang, R. J., Magleby, S., and Howell, L., 2015. “Single degree-of-freedom rigidly foldable origami flashers”. *ASME Paper No. DETC2015-46961*.

[46] http://www.kjmagnetics.com/.

[47] Griffiths, D. J., 1962. *Introduction to electrodynamics*. Prentice Hall.

[48] Lang, R. J., Tolman, K. A., Crampton, E. B., Ma gleby, S. P., and Howell, L. L., 2018. “A review of thickness-accommodation techniques in origami inspired engineering”. *Applied Mechanics Reviews, 70*(1), p. 010805.

Material Systems and Structures, 27(15), pp. 2049–2061.

[39] Guitron, S., Guha, A., Li, S., and Rus, D., 2017. “Autonomous locomotion of a miniature, untethered origami robot using hall effect sensor-based mag netic localization”. In Robotics and Automation (ICRA), 2017 IEEE International Conference on, IEEE, pp. 4807–4813.

[40] Salerno, M., Zuliani, F., Firouzeh, A., and Paik, J., 2017. “Design and control of a low profile electromag netic actuator for foldable pop-up mechanisms”. *Sen sors and Actuators A: Physical*.

[41] Hernandez, E. A. P., Hartl, D. J., Malak, R. J., Akle man, E., Gonen, O., and Kung, H.-W., 2016. “Design tools for patterned self-folding reconfigurable struc tures based on programmable active laminates”. *Jour nal of Mechanisms and Robotics, 8*(3), p. 031015.

[42] Hawkes, E., An, B., Benbernou, N. M., Tanaka, H., Kim, S., Demaine, E. D., Rus, D., and Wood, R. J., 2010. “Programmable matter by folding”. *Proceedings of the National Academy of Sciences*.

[43] Bowen, L., Springsteen, K., Feldstein, H., Frecker, M., and Simpson, T., 2014. “A dynamic model of magneto active elastomer actuation of the waterbomb base”. *Journal of Mechanical Design*.

[44] Sheridan, R., Roche, J., Lofland, S., and von Lockette, P., 2014. “Numerical Simulation and experimental vali